Food Control 131 (2022) 108412

Contents lists available at ScienceDirect

Food Control

journal homepage: www.elsevier.com/locate/foodcont

Evaluation of the effect of factors related to preparation and composition of grated Parmigiano Reggiano cheese using NIR hyperspectral imaging

R. Calvini [a], S. Michelini [b], V. Pizzamiglio [b], G. Foca [a,c], A. Ulrici [a,c,*]

[a] Department of Life Sciences, University of Modena and Reggio Emilia, Pad. Besta, Via Amendola, 2, Reggio Emilia, 42122, Italy
[b] Parmigiano Reggiano Cheese Consortium, Via J.F. Kennedy, 18, Reggio Emilia, 42121, Italy
[c] Interdepartmental Centre BIOGEST-SITEIA, University of Modena and Reggio Emilia, Piazzale Europa, 1, Reggio Emilia, 42122, Italy

ARTICLE INFO

Keywords:
NIR hyperspectral Imaging
ANOVA Simultaneous component analysis
Multivariate image analysis
Data dimensionality reduction
Parmigiano Reggiano cheese

ABSTRACT

The present study is focused on the evaluation of the effect of grater type and fat content of the pulp on the spectral response obtained by near infrared hyperspectral imaging (NIR-HSI), when this technique is used to determine the rind percentage in Parmigiano Reggiano (P-R) cheese.

To this aim, grated P-R cheese samples were prepared considering all the possible combinations between three levels of rind amount (8%, 18% and 28%), two levels of fat content of the pulp and two different grater types, and the corresponding hyperspectral images were acquired in the 900–1700 nm spectral range. In a first step, the average spectrum (AS) was calculated from each hyperspectral image, and the corresponding dataset was analysed by means of Analysis of Variance Simultaneous Component Analysis (ASCA) to assess the effect of the three considered factors and their two-way interactions on the spectral response. Then, the hyperspectral images were converted into Common Space Hyperspectrograms (CSH), which are signals obtained by merging in sequence the frequency distribution curves of quantities calculated from a Principal Component Analysis (PCA) model common to the whole hyperspectral image dataset. ASCA was also applied to the CSH dataset, in order to evaluate the effect of the considered factors on this kind of signals.

Generally, all the three factors resulted to have a significant effect, but with a different extent according to the method used to analyse the hyperspectral images. Indeed, while fat content of the pulp and rind percentage showed a comparable effect on the spectral response of AS dataset, in the case of CSH signals rind percentage had a greater effect compared to the other main factors. However, CSH were also more sensitive to differences ascribable to the natural variability between diverse Parmigiano Reggiano cheese samples.

1. Introduction

The Protected Designation of Origin (PDO) applied to Parmigiano Reggiano (P-R) cheese is also extended to grated cheese products obtained by P-R cheese wheels, under the condition that the product is grated in the specific production area and packaged immediately afterwards, in order to maintain its organoleptic properties.

All the stages of P-R production are regulated by the Specifications of Parmigiano Reggiano Cheese (https://www.parmigianoreggiano.com/consortium/rules_regulation_2/default.aspx), which also define the requirements of grated P-R cheese products. Among these, a maximum value is set for the rind percentage (RP) in grated P-R cheese, which should not exceed the 18% (w/w) value.

In the frame of the implementation of fast and non-destructive methods to assess quality compliance of cheese products (Alinovi et al., 2019; Cevoli et al., 2013; Lei & Sun, 2019; Li Vigni et al., 2020), in a previous study we evaluated the potential of Near Infrared Hyperspectral Imaging (NIR-HSI) in the determination of rind percentage in grated Parmigiano Reggiano cheese (Calvini, Michelini, et al., 2020). NIR-HSI allows to combine the advantages of NIR spectroscopy and of imaging techniques, to obtain spectral and spatial information from a sample. Indeed, hyperspectral images (also named *hypercubes*) are three-dimensional data arrays with two spatial dimensions (x pixel rows and y pixel columns), accounting for pixel location on the sample surface, and one spectral dimension, corresponding to the λ wavelengths acquired in a specific spectral range (Amigo et al., 2015; Gowen et al., 2007, 2008).

Thanks to the possibility of coupling both spectral and spatial

* Corresponding author. Department of Life Sciences, University of Modena and Reggio Emilia, Pad. Besta, Via Amendola, 2, Reggio Emilia, 42122, Italy.
E-mail address: alessandro.ulrici@unimore.it (A. Ulrici).

https://doi.org/10.1016/j.foodcont.2021.108412
Received 22 February 2021; Received in revised form 9 June 2021; Accepted 6 July 2021
Available online 7 July 2021

information, the applications of NIR-HSI are continuously growing in different research and technical areas, including food quality control (Huang et al., 2014; Lorente et al., 2012; Shan et al., 2020; Wu & Sun, 2013), implementation of online sorting systems for waste management (Bonifazi et al., 2018; Calvini et al., 2018), pharmaceutical analysis (Roggo et al., 2005), and many others (Caballero et al., 2020; Calvini, Ulrici, & Amigo, 2020). Thus, NIR-HSI is particularly suitable for the analysis of heterogenous food matrices, like P-R grated cheese samples, which are composed by particles derived from both cheese pulp and rind with different chemical and physical properties.

In order to extract the relevant information from hyperspectral images, it is mandatory to apply proper data analysis strategies based on multivariate statistics (Duchesne et al., 2012; Prats- Montalbán et al., 2011). Furthermore, in practical applications of HSI it is often necessary to acquire a large number of hyperspectral images of different samples and to simultaneously analyse them to gain a comprehensive overview of the whole image dataset. In this case, it is necessary to reduce the relevant information contained in each three-dimensional hypercube into a feature vector, by means of proper data-dimensionality reduction methods. These feature vectors are then collected into a data matrix, which in turn can be analysed using common chemometric methods (Calvini et al., 2016; Kucheryavskiy, 2013; Oliveri et al., 2019).

The most common approach of data dimensionality reduction consists in calculating the average spectrum from each hyperspectral image of the dataset. This simple method is very effective for summarizing the overall spectral information of the sample, but it involves the loss of information about the variability between the single pixel-spectra of the image.

For this reason, alternative methods have been proposed to retain also the information related to spatial variability within the images, such as the *hyperspectrograms* approach. This method consists in converting each hyperspectral image into a vector obtained by merging in sequence the frequency distribution curves of quantities obtained from a PCA model, named Common Space Hyperspectrogram (CSH) (Calvini et al., 2016; Corti et al., 2017; Ferrari et al., 2013, 2015; Xu et al., 2016).

In our previous study related to the application of NIR-HSI to determine rind percentage in grated P-R products, hyperspectral images of grated P-R cheese samples with varying levels of rind percentage were acquired in the 900–1700 nm spectral range (Calvini, Michelini, et al., 2020). The hyperspectral images were converted into the corresponding CSH signals, which were used to calculate a calibration model to estimate the RP values. The satisfactory results suggested the effectiveness of the proposed approach in the determination of the RP values. However, before extending this method to a practical application, it is necessary to estimate the effect of the main variability sources involved in the production of grated P-R cheese. Based on this consideration, in agreement with the Parmigiano Reggiano Cheese Consortium, in the present study we focused on fat content of the pulp and on grater type as the main factors potentially affecting the spectral response obtained by NIR-HSI in the determination of rind amount in grated P-R cheese.

Due to the artisanal nature of Parmigiano Reggiano, the fat content of the cheese wheels shows a variable trend (Cevoli et al., 2015; Panari et al., 2003), which in turn influences rheological, mechanical, and textural properties of the product (Guinee et al., 2000; Rogers et al., 2010).

In addition, producers can prepare the grated P-R cheese products using two types of graters: knife mill and drum grater, which produce particles with different shape and dimensions. For this reason, the hyperspectral images of grated cheese samples can be influenced by the different physical properties of cheese particles due to grater type.

Therefore, fat content of the pulp and granulometry of cheese particles modify the spectral response obtained by NIR-HSI, and these factors may affect the calibration models able to predict rind percentage from NIR hyperspectral images of grated P-R cheese.

Based on these considerations, in this study grated P-R cheese samples were prepared according to a Design of Experiments (DOE) approach (Granato & de Araújo Calado, 2014), which allows to strategically plan the experiments by selecting only the samples relevant to describe the whole experimental domain. In particular, all the possible combinations between three levels of rind percentage (w/w), two levels of fat content of the pulp, and the two grater types were considered. The corresponding hyperspectral images were converted to both average spectra (AS) and CSH, which were analysed by means of ANOVA Simultaneous Component Analysis (ASCA). This method, which essentially consists of the generalization of ANOVA to the analysis multivariate datasets, was used to investigate the extent of the effect of the considered factors (i.e., rind percentage, fat content and grater type) and of their interactions on the spectral response.

2. Material and methods

2.1. Experimental design and cheese samples

The grated cheese samples considered in the present study were provided by Parmigiano Reggiano cheese Consortium and prepared according to the following three-factor full factorial design:

1. Fat content of the pulp, with two levels: pulp with high fat content (range: 47.0%–48.8%) and pulp with low fat content (range: 43.0%–44.0%);
2. Grater type, with two levels: drum grater and knife mill;
3. Rind percentage, with three levels: 8%, 18% and 28%.

Based on a DOE approach, 12 mixtures of grated cheese were identified according to a three-factor full factorial design, corresponding to all the possible combinations between the experimental factors (3 levels of rind percentage $\times$ 2 levels of fat content of the pulp $\times$ 2 levels of grater type). It has to be highlighted that these mixtures were selected in a manner to be representative of the whole experimental domain.

The grated cheese samples were provided by Parmigiano Reggiano cheese Consortium and three measurement sessions were planned on different days (A, B and C), preparing for each session the 12 grated cheese mixtures. In this manner, a total of 36 grated cheese samples were considered.

Therefore, the mixtures identified using the DOE approach were repeated three times since in each session the samples were prepared starting from different cheese wheels matured for a period of 12 months. In particular, for each session two batches of Parmigiano Reggiano cheese, one with high fat content and one with low fat content, were used to obtain the rind and pulp pieces. Considering the pulp batches with high fat content, the corresponding fat percentages were equal to 47.1%, 48.9% and 47.0% for sessions A, B and C, respectively; while for the low-fat pulp matrices, the corresponding fat content was equal to 43.0%, 44.0% and 43.9% for sessions A, B and C, respectively.

Then, the pieces of pulp and rind were grated with the two grater types. When using the knife mill (Grindomix GM 200, Retsch), cheese pulp was grated for 15 s with a speed equal to 4500 rpm, while cheese rind was grated for 30 s at a speed equal to 8500 rpm. Considering the drum grater, the samples were grated using a Ghizzoni mod. GS electric grater.

Finally, the matrices of pulp and rind were used to obtain the mixtures with 8%, 18% and 28% (w/w) of rind. All the mixtures were further grated with the knife mill for 15 s at a speed of 4500 rpm in order to ensure homogeneous distribution of rind and pulp particles within each sample.

The samples, each one consisting of 100 g of grated cheese, were stored in the dark at 4 °C, and were delivered to the laboratory the next day, where hyperspectral images were immediately acquired.

2.2. Image acquisition and elaboration

During each measurement session three aliquots of about 13 g of

grated cheese were collected from each sample and positioned in a plastic Petri dish with a diameter equal to 5.5 cm. The hyperspectral images were acquired in a manner to include in the image scene the three aliquots of two samples randomly selected among those delivered for the measurement session, and 6 hyperspectral images were acquired in each session, for a total of 18 hyperspectral images over the three sessions. In each image, the plastic Petri dishes containing the three aliquots of two samples were placed according to a 3 × 2 chessboard scheme on a black silicon carbide sandpaper, used as background during image acquisition. The image scene also included a high reflectance white ceramic tile (99% reflectance) and two ceramic tiles with intermediate reflectance values (89% and 46%, respectively).

The hyperspectral image acquisition system (NIR Spectral Scanner, DV Optic) worked with a line-scanning configuration and consisted of a Specim Imspector N17E Imaging spectrometer coupled to a Xenixs Xeva-1.7-320 camera (320 × 256 pixels) embedding Specim Oles 31 f/2.0 optical lens.

The hyperspectral images were acquired in the 900–1700 nm spectral range with a spectral resolution of 5 nm. However, due to the low signal-to-noise ratio at the edges of the spectral range, only the 131 spectral channels between 1000 nm and 1650 nm were kept for further analysis.

The measure of the high reflectance reference was used, together with the measure of the dark current, to convert the raw detector counts into reflectance values. Furthermore, the images were also subjected to an additional internal calibration procedure which corrects each image of the dataset by comparing the average reflectance values of the ceramic tiles and of the dark current with those measured on an image chosen as reference (Ulrici et al., 2013).

In order to have a single image for each sample aliquot, the corrected images were then cropped and a total of 108 images were obtained (= 36 grated cheese samples × 3 aliquots).

Subsequently, the pixels of the sandpaper background were excluded from each image by setting a threshold at 1100 nm wavelength. More in detail, only the pixels with a reflectance value measured at 1100 nm higher than 0.5 reflectance units were considered for further analysis, since they were ascribable to the grated cheese, while the remaining pixels were ascribable to the black sandpaper background or to the plastic Petri dish. In addition, also the pixels located at the edges of the region of interest obtained after background removal were excluded by applying a morphological erosion using a disk-shaped structuring element with radius equal to 8 pixels (Van Den Boomgaard & Van Balen, 1992).

The procedures for image acquisition and elaboration described in this section were optimised in our previous study related to the quantification of rind percentage in Parmigiano Reggiano grated cheese, therefore further details about these aspects can be found in Calvini, Michelini, et al., 2020.

The image elaboration procedures (i.e., image correction, background removal and morphological erosion) were performed in MATLAB environment (ver. 9.3, The Mathworks Inc., USA) using routines written *ad hoc*.

2.3. Data dimensionality reduction of the hyperspectral images

2.3.1. Average spectra

From each image of the dataset the average spectrum was calculated considering only the spectra of the retained pixels. The average spectra (AS) were then stored into a matrix with 108 rows, corresponding to the number of images, and 131 columns, corresponding to the spectral channels. Fig. 1 shows the spectra of the AS dataset coloured according to grater type, fat content of the pulp and rind percentage of the corresponding samples.

2.3.2. Common Space Hyperspectrograms

The hyperspectral images were also converted into Common Space

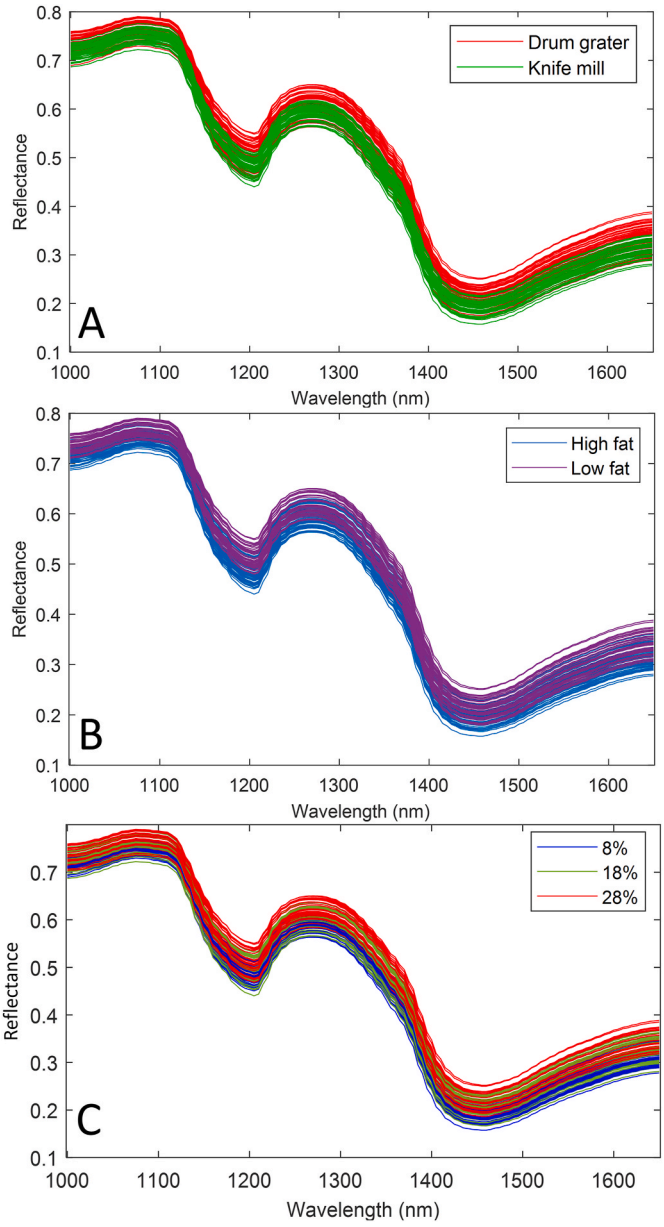

Fig. 1. AS dataset: the spectra are coloured according to grater type (A), fat content of the pulp (B) and rind percentage (C) of the corresponding samples.

Hyperspectrograms (CSH), which are signals obtained by merging in sequence the frequency distribution curves of quantities derived from a PCA model common to all the images of the dataset (Calvini et al., 2016).

In the first step of the calculation of the CSH signals, the three-dimensional hyperspectral images were unfolded into data matrices with as many rows as the number of pixels kept after image elaboration (i.e., background removal and morphological erosion) and as many columns as the number of wavelengths. Then, based on a preliminary analysis of the average spectra, Standard Normal Variate (SNV) was applied as row-wise preprocessing method of the unfolded hypercubes, and the preprocessed spectra were finally centered according to the global mean spectrum, i.e., by subtracting the mean spectrum obtained averaging all the retained pixel spectra of all the hyperspectral images of the dataset.

Subsequently, a PC space common to all the images of the dataset was calculated by means of singular value decomposition (SVD) of the kernel variance-covariance matrix, computed as the sum of the single

variance-covariance matrices of each preprocessed and unfolded hypercube. In particular, the global PCA model was calculated considering 3 principal components.

Finally, for each hyperspectral image, the corresponding CSH was calculated by merging in sequence the frequency distribution curves of the three score vectors obtained by projecting the image onto the global PC space. The frequency distribution curves were calculated using a number of bins equal to 150, therefore the hyperspectrogram of each image is a vector of length equal to 450 points (= 3 PCs × 150 bins). In addition, the frequency distribution curves of each image were normalised according to the number of pixels kept after background removal and erosion, in order to account for the fact that every image has a different number of retained pixels.

Therefore, the resulting CSH data matrix has 108 rows, corresponding to the number of images, and 450 columns, corresponding to the hyperspectrogram variables.

Usually, the frequency distribution curves of Hotelling's T^2 values and Q residuals are also included at the end of the CSH signals. However, a preliminary investigation of the CSH dataset calculated in the conventional manner allowed to highlight that the hyperspectrogram regions related to Hotelling's T^2 values and Q residuals were strongly affected by unwanted variations caused by the illumination system. For these reasons, in this study only the frequency distribution curves of the score vectors were included in the CSH signals.

The conversion of the hyperspectral images into CSH signals was performed using Hyperpectrograms GUI, a MATLAB-based graphical user-friendly interface, freely downloadable from http://www.chimslab.unimore.it/downloads/, developed by some of the Authors and derived from a similar software for the analysis of RGB images (Calvini, Orlandi, et al., 2020).

Fig. 2 shows the hyperspectrograms of the CSH dataset coloured according to grater type, fat content of the pulp and rind percentage of the corresponding samples.

2.4. Data analysis

ASCA is a chemometric method specifically developed to analyse multivariate datasets resulting from designed experiments, and it can be considered as an extension of ANOVA from univariate to multivariate data, which allows to interpret the variation induced by the different design factors (De Luca et al., 2016; Jansen et al., 2005; Smilde et al., 2005).

Like ANOVA, ASCA is based on the assumption that the response matrix obtained from a designed experiment can be decomposed in different *effect matrices*, which account for the influence of the experimental factors and of their interactions. In the specific case under investigation, the mean centered data matrices of AS or CSH signals ($\overline{\mathbf{X}}$) can be partitioned into the matrices accounting for the variability induced by the effect of grater type ($\mathbf{X_{grater}}$), fat content of the pulp ($\mathbf{X_{fat}}$) and rind percentage ($\mathbf{X_{rind}}$) as main factors, and of their two-way interactions ($\mathbf{X_{grater \times fat}}$, $\mathbf{X_{fat \times rind}}$, $\mathbf{X_{grater \times rind}}$). In addition, the residuals matrix ($\boldsymbol{E}$) is also calculated, which accounts for the variability not included in the ASCA model, as schematized in Fig. 3.

The effect matrix of each factor has as many rows as the number of samples, and all the rows corresponding to samples belonging to the same factor level contain the average response of the considered level. For example, in the $\mathbf{X_{grater}}$ matrix calculated from the CSH dataset all the rows corresponding to samples grated with the knife mill contain the average signal of this level, obtained by averaging all the mean centered hyperspectrograms of samples processed with the knife mill.

The effect matrices of the interactions are calculated in the same manner after a deflation step, i.e., after subtracting from $\overline{\mathbf{X}}$ the effect matrices of the main factors.

Then, PCA is applied to each effect matrix, obtaining a PCA submodel for each factor, for each interaction and for the residual matrix $\mathbf{E}$.

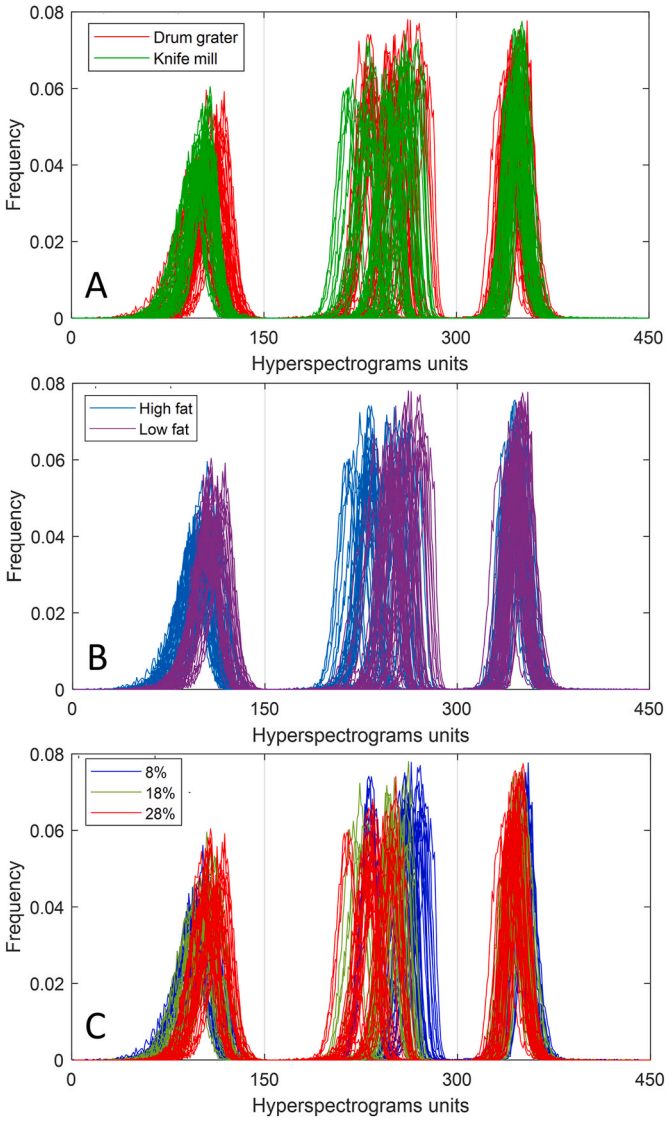

Fig. 2. CSH dataset: the signals are coloured according to grater type (A), fat content of the pulp (B) and rind percentage (C) of the corresponding samples.

Therefore, each matrix resulting from ANOVA partitioning is decomposed by means of PCA as follows:

$$\boldsymbol{X}_k = \boldsymbol{T}_k \boldsymbol{P}_k^T + \boldsymbol{E}_k \quad (1)$$

where $\boldsymbol{X}_k$ represents the k-th effect matrix, $\boldsymbol{T}_k$ and $\boldsymbol{P}_k^T$ represent the corresponding score and loading matrices, and $\boldsymbol{E}_k$ is the corresponding residual matrix.

These PCA submodels maximize the differences between level averages of each effect matrix $\boldsymbol{X}_k$, without considering the variability within samples belonging to the same level.

In order to compare the magnitude of the differences between factor levels with the residual variability, the effect matrix can be summed with the ASCA residual matrix $\boldsymbol{E}$, and the resulting ($\boldsymbol{X}_k + \boldsymbol{E}$) matrix is then projected onto the $\boldsymbol{P}_k$ loading space:

$$\boldsymbol{T}_{X_k+E} = (\boldsymbol{X}_k + \boldsymbol{E})\boldsymbol{P}_k \quad (2)$$

The score matrix $\boldsymbol{T}_{X_k+E}$ obtained from Eq. (2) allows to evaluate the residual variability in the PC subspace of factor k (Zwanenburg et al., 2011).

When dealing with the interaction terms, the interpretation of the PCA submodels calculated as expressed in Equations (1) and (2) is

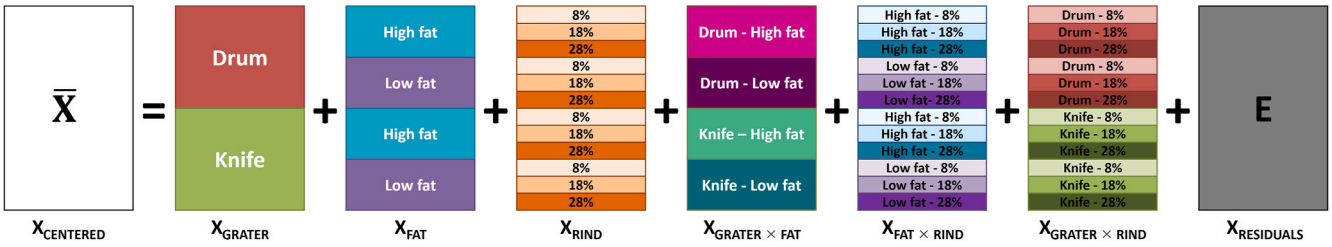

Fig. 3. Schematic representation of ASCA decomposition of AS and CSH datasets.

generally not intuitive, since these models represent the deviation of a particular combination of levels from the overall effects of the corresponding factors. To overcome this issue, the PCA model can be calculated on the matrix obtained by summing the two effect matrices of the single factors and the effect matrix of the corresponding interaction (Bertinetto et al., 2020).

The extent of the contribution of each factor or interaction can be expressed using the sum of squares of the elements of the corresponding effect matrix:

$$SSQ_k = X_k^2 \tag{3}$$

where SSQ_k is the sum of squares of the effect matrix $\boldsymbol{X}_k$ of factor k.

The significance of an effect can be assessed by comparing SSQ_k with the distribution of values corresponding to the null hypothesis (i.e., the considered effect has no significance), which can be non-parametrically estimated using a permutation test. If SSQ_k is systematically larger than the values of such a null distribution with a defined significance level, the tested effect can be considered as statistically significant. In this study, the permutation test was performed considering 1000 permutations and a significance level equal to 0.05.

Before data analysis using ASCA, the AS dataset was preprocessed using SNV and mean centering, while the CSH dataset was preprocessed using mean centering.

Data preprocessing and data analysis with ASCA were performed using the PLS_Toolbox software (v. 8.8.1) running under MATLAB environment.

3. Results and discussion

3.1. ASCA of average spectra dataset

The application of ASCA to the mean centered **AS** matrix allowed to partition the variability of the dataset into seven matrices accounting for the effect of the three main factors ($\mathbf{AS_{grater}}$, $\mathbf{AS_{fat}}$, $\mathbf{AS_{rind}}$), their two-way interactions ($\mathbf{AS_{grater\times rind}}$, $\mathbf{AS_{grater\times fat}}$, $\mathbf{AS_{fat\times rind}}$) and the residuals ($\mathbf{AS_{RESIDUALS}} = \mathbf{E}$). The percentage of variance retained by each matrix resulting from ASCA partitioning of the AS dataset is reported in the second column of Table 1. All the three main factors resulted to have a significant effect on the spectral response, while considering their two-way interactions only the interaction between grater type and fat content of the pulp was not significant based on the permutation test.

Table 1
Results obtained from ASCA applied to AS dataset and CSH dataset: for each dataset, the corresponding column reports the percentage of variance explained by each factor.

Factor	AS dataset	CSH dataset
Grater type	14.85%	4.70%
Fat content	30.21%	11.69%
Rind percentage	30.34%	19.68%
Grater × Fat	0.36% *	1.83%
Grater × Rind	4.67%	3.05%
Fat × Rind	1.97%	5.58%
Residuals	17.60%	53.47%

* not significant term ($p > 0.05$).

Fat content and rind percentage are the factors with the greatest effect on the spectral response, with a comparable effect in terms of explained data variance, each one accounting for about 30% of total variability.

The results of the PCA submodel related to rind percentage ($\mathbf{AS_{rind}}$) are reported in Fig. 4A and Fig. 4B. In particular, this model allows to evaluate the effect of rind percentage on the spectral response regardless of the other considered factors, i.e., of fat content and grater type, by projecting onto the submodel loading space the effect matrix $\mathbf{AS_{rind}}$ summed with the ASCA residuals matrix **E**, as defined in equation (2). Comparing the score plot in Fig. 4A with the corresponding loading vector reported in Fig. 4B, it is possible to observe that the samples with the highest amount of rind are located at positive PC1 score values, and that positive loading values can be found in the spectral region falling in the 1320–1390 nm wavelength range, which includes the C–H bond combination band, ascribable to lipids (Burns & Ciurczak, 2008, chap. 17, pp. 356–357; Šašić & Ozaki, 2000). In the same manner, the samples with RP values equal to 8% are placed at negative PC1 score values, and negative PC1 loading values can be found in the spectral regions centered at 1070 nm, corresponding to the N–H bond first overtone (proteins) and in the spectral region falling in the 1420–1520 nm, which includes the first overtone of O–H and N–H bonds, ascribable to the presence of bound water and proteins (Ozaki, 2002). For a proper evaluation of these outcomes it must be recalled that the spectra were acquired in reflectance mode: increasing reflectance values correspond to decreasing absorbance values, thus to decreasing concentrations of the chemical species absorbing in the relevant spectral bands.

Therefore, the interpretation of PC1 scores and loadings suggests that samples with higher amount of cheese rind have higher protein content and higher levels of bound water, while samples with lower rind percentage have a higher amount of fat. As pointed out by previous studies, the differences in composition between the inner and the outer part of cheese wheels are mainly due to the centripetal trend of biochemical processes occurring during maturation, such as dehydration, lipolysis and proteolysis (Alinovi et al., 2019; Malacarne et al., 2009; Malegori et al., 2021; Priyashantha et al., 2020).

In order to investigate the interaction between grater type and rind percentage, the corresponding PCA submodel was calculated considering the matrix obtained by summing $\mathbf{AS_{GRATER}} + \mathbf{AS_{RIND}} + \mathbf{AS_{GRATER\times RIND}}$ ($\mathbf{AS_{GRATER\ +\ RIND\ +\ GRATER\times RIND}}$) for a better interpretability of the results. Following the same procedure described in Section 2.4 for the main factors, also in this case the ($\mathbf{AS_{GRATER\ +\ RIND\ +\ GRATER\times RIND}} + \mathbf{E}$) matrix was projected onto the PC subspace obtained from the decomposition of $\mathbf{AS_{grater\ +\ rind\ +\ grater\times rind}}$, to evaluate also the sample variability associated with the two factors and their interaction.

The corresponding PC1 score plot is reported in Fig. 4C. In this case PC1 describes the variability associated with the different levels of rind percentage. It can be observed that the samples grated with the drum grater (represented with triangles) show a greater variation depending on the RP values with respect to those grated with the knife mill (represented with circles). This behaviour could be explained by considering the effect of different particle sizes on the spectral response, due to scattering phenomena.

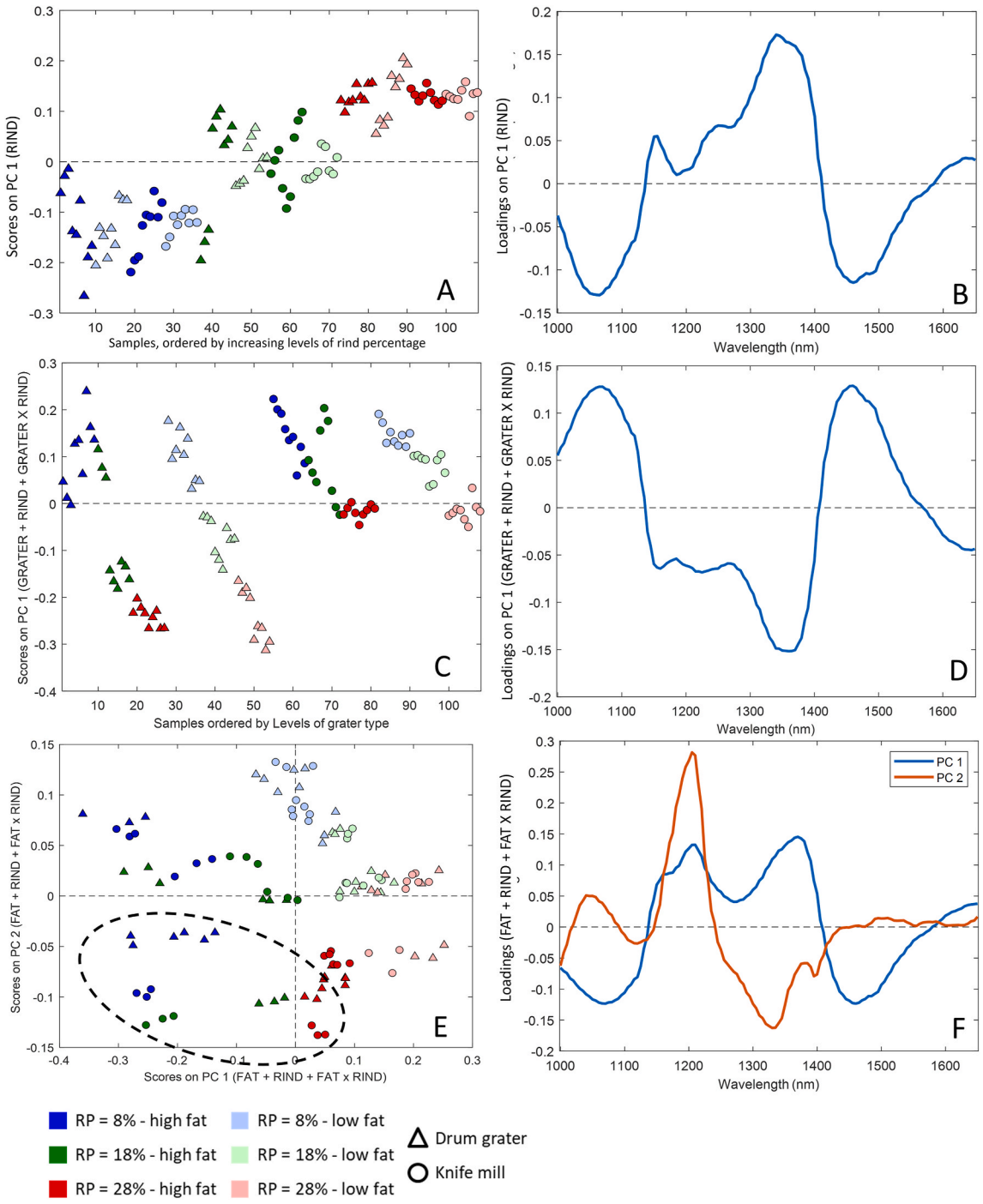

Fig. 4. ASCA results obtained from AS dataset: scores of projected effect plus residuals matrix (A) and loading vector (B) of the PCA submodel calculated from the $\mathbf{AS}_{\text{RIND}}$ effect matrix; scores of projected effects plus residuals matrix (C) and loading vector (D) of the PCA submodel calculated from the $\mathbf{AS}_{\text{GRATER + RIND + GRATER×RIND}}$ matrix; scores of projected effects plus residuals matrix (E) and loading vectors (F) of the PCA submodel calculated from the $\mathbf{AS}_{\text{FAT + RIND + FAT×RIND}}$.

Alinovi et al. (2019) used image analysis to evaluate size and shape differences of cheese particles obtained by grating the inner and outer parts of P-R cheese wheels using a drum grater. Their study showed that grated rind is characterized by finer particles with a fibrous shape, while grated pulp has particles with a more spherical shape. This behaviour is due to the different mechanical properties of P-R rind and pulp, which in turn are mainly influenced by the differences in moisture content of inner and outer parts of the cheese wheel (Campbell et al., 2007; Haddad et al., 1999). The effect of a knife mill on cheese particles has not been reported in literature, however grater type could affect size and shape of the particles. In particular, drum graters tend to produce more elongated particles, while knife mills tend to produce particles with a regular round shape (Paulrud et al., 2002). Given these considerations, we suppose that the difference in shape between rind and pulp particles is less pronounced when the cheese is grated with the knife mill, resulting in a lower variation of the spectral response with varying RP values, as observed in Fig. 4C.

The effect of grater type is more evident on rind particles and, for this reason, in Fig. 4C the difference between samples prepared with the two grater types is not evident when the amount of rind is low (samples reported in blue colour correspond to 8% RP values), while it becomes clearly visible with increasing rind percentages (samples reported in

green and red colour correspond to 18% and 28% RP values, respectively).

The PC1 loading plot of this model is reported in Fig. 4D, which clearly resembles the loading plot of the previous model (Fig. 4B), but with opposite sign. This confirms that PC1 essentially describes the effect of RP rather than the effect of grater type, consistent with the higher percentage of variance accounted for by RP with respect to the percentage of variance accounted for by grater type (Table 1).

In the same manner, to evaluate the interaction between fat content of the pulp and rind percentage, the corresponding PCA submodel was calculated considering the $\mathbf{AS_{fat\ +\ rind\ +\ fat\times rind}}$ matrix (resulting from the sum of $\mathbf{AS_{fat}}$, $\mathbf{AS_{rind}}$ and $\mathbf{AS_{fat\times rind}}$), and then the ($\mathbf{AS_{grater\ +\ rind\ +\ grater\times rind}}$ + **E**) matrix was projected onto the PC subspace. The corresponding PC1-PC2 score plot is reported in Fig. 4E, where it is possible to observe that objects displacement is related both with rind percentage and with fat content. In particular, moving from the upper right to the lower left corner of the graph the samples are generally arranged according to increasing fat content, while moving from the upper left to the lower right corner of the graph the samples vary according to their RP value. Generally, the cheese samples with a low amount of fat (light colours) are more grouped and present a more regular trend according to rind percentage, with respect to the samples with a high amount of fat. In particular, it is possible to observe the peculiar behaviour of the group of samples with high fat content that have been inscribed in the ellipse in Fig. 4E. Indeed, all these samples lie at lower PC2 values with respect to the other high-fat content samples with the same RP values. For example, the samples inscribed in the ellipse with RP = 8% and high fat content (dark blue symbols) lie at lower PC2 values with respect to the other high fat content samples with the same RP value, i.e., with respect to the other samples represented with dark blue symbols that lye at positive values of PC2. It was found that the samples inscribed in the ellipse were imaged in the second measurement session. Recalling that for each measurement session two different cheese wheels were used, one with a low and one with a high fat content, it must be underlined that Parmigiano Reggiano cheese is an artisanal product, thus the "high fat" and the "low fat" levels do not correspond to two fixed values, but to two distinct fat content ranges. Therefore, the position in the PC1-PC2 score plot of the high-fat content samples of the second measurement session suggests that they were prepared from a cheese wheel with a higher fat content, compared to the samples of the other measurement sessions. Indeed, the high-fat content samples of the second measurement session were prepared from a cheese wheel with a fat content equal to 48.9%, that was significantly higher than the value measured on the cheese wheels used for the other two sessions (47.1% and 47.0%).

A similar behaviour is also observed for a group of low-fat content samples with RP value equal to 28%, which correspond to those measured during the third session, and that show lower PC2 values compared to the similar samples.

In accordance with these considerations, the residuals account for 17.60% of data variability, which is greater than the effect of grater type factor (14.85%). This is due to the fact that the residuals mainly account for the differences between diverse measurement sessions, which in turn essentially consider the variability between the different cheese wheels, coming from different cheese factories.

Concerning the PC1-PC2 loading plot reported in Fig. 4F, the PC1 loading vector is similar to the corresponding vector reported in Fig. 4B, but with a higher positive contribution of the spectral region centered at about 1210 nm, corresponding to the C–H bond second overtone (Burns & Ciurczak, 2008, chap. 17, pp. 356–357; Šašić & Ozaki, 2000). The same spectral region is also the one that provides the main positive contribution to the PC2 loading vector, which is consistent with the fact that the samples with the highest fat content are found at negative values of both PC1 and PC2 in Fig. 4E.

3.2. ASCA of CSH dataset

In our previous study to evaluate the feasibility of using NIR-HSI to determine the rind percentage in grated Parmigiano Reggiano cheese samples (Calvini, Michelini, et al., 2020), the calibration models were calculated starting from the CSH signals of the hyperspectral images. In order to evaluate the effect of the considered factors on these signals, ASCA was also applied to the CSH matrix obtained from the hyperspectral images acquired in this study, and the corresponding results are reported in the last column of Table 1. Interestingly, the residuals account for 53.47% of data variance; a further investigation of this effect through the corresponding PCA submodel allowed to verify that the residuals mainly describe the peculiar behaviour of some samples, in particular those analysed in the second measurement session, as previously outlined in the discussion of the ASCA submodel of $\boldsymbol{AS_{FAT\ +\ RIND\ +\ FAT\times RIND}}$ matrix (Section 3.1, Fig. 4E and F).

Among the main experimental factors, rind percentage has the highest effect, accounting for 19.68% of data variance, followed by fat content (11.69%) and grater type (4.70%). The results of the PCA submodel related to the effect matrix $\mathbf{CSH_{rind}}$ (that was analysed in the same manner as it was previously done for $\mathbf{AS_{rind}}$ in Section 3.1) are reported in Fig. 5A. In the PC1 score plot (Fig. 5A) it is possible to observe that the CSH signals are displaced according to the extreme levels (8% and 28%) of RP values of the cheese samples, while the samples with RP equal to 18% have mainly PC1 values equal to those of the samples with RP equal to 28%. The corresponding PC1 loading vector (data not shown for conciseness reasons) showed that the major contribution to this separation is given by the CSH regions related to PC2 of the global PCA model and reflects the shift of the peaks of the CSH signals related to different RP values, as reported in Fig. 2C.

Considering the two-way interactions, all interactions resulted to be significant in the ASCA model, but the FAT × RIND interaction has a greater effect (5.58% of data variance) compared to GRATER × RIND and GRATER × FAT interactions.

To better evaluate the effect of FAT × RIND interaction, the corresponding PCA submodel was calculated considering the matrix obtained by summing $\mathbf{CSH_{GRATER}}$ + $\mathbf{CSH_{RIND}}$ + $\mathbf{CSH_{GRATER\times RIND}}$ ($\mathbf{CSH_{GRATER\ +\ RIND\ +\ GRATERXRIND}}$) and then the ($\mathbf{CSH_{GRATER\ +\ RIND\ +\ GRATERXRIND}}$ + **E**) matrix was projected onto the so-obtained PC subspace, following the same procedure previously described in Section 3.1 for the AS dataset. In this case, PC1 mainly describes the variation ascribable to the different rind percentage levels (Fig. 5B). Concerning the high-fat content samples, it is possible to observe a group (inscribed in the ellipse in Fig. 5B) that lies at lower PC1 values with respect to the other high-fat content samples with the same RP values, corresponding to the same samples already discussed in Section 3.1 (Fig. 4E). Similarly, the same group of low-fat content samples with RP value equal to 28% that in were found at low PC2 values in Fig. 4E is found at low PC1 values also in Fig. 5B, suggesting that the use of two completely different data dimensionality reduction approaches such as AS and CSH showed a similar ability to identify differences between samples coming from different cheese wheels.

4. Conclusions

This study of NIR hyperspectral images of grated Parmigiano Reggiano cheese was aimed at evaluating the effect on the spectral response of three factors, namely grater type, rind percentage and fat content of the pulp. The grated P-R cheese samples were prepared according to a full factorial design, and the corresponding hyperspectral images were then converted in signals by means of two data dimensionality reduction methods, i.e., average spectra (AS) and Common Space Hyperspectrograms (CSH). This allowed to evaluate the effect on the spectral response of the three considered factors and of their interactions by analysing with ASCA both the AS and the CSH datasets.

The analysis of both the datasets revealed that all the considered

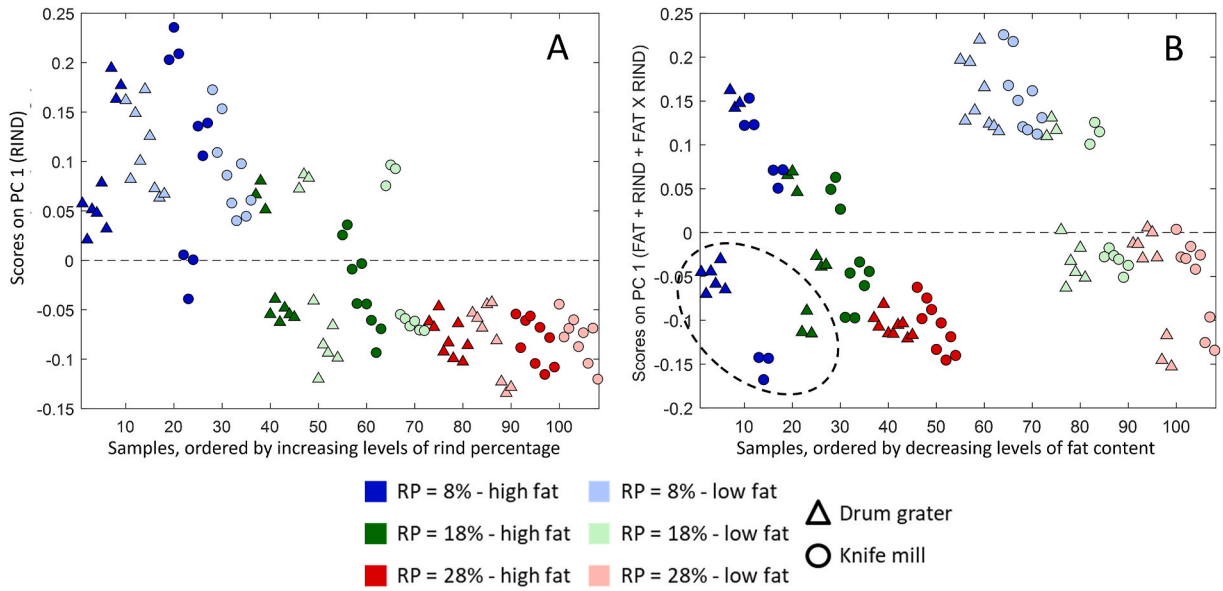

Fig. 5. ASCA results obtained from CSH dataset. Scores of projected effect plus residuals matrix of the PCA submodel calculated from the $\mathbf{CSH}_{\mathrm{RIND}}$ effect matrix (A) and scores of projected effect plus residuals matrix of the PCA submodel calculated from the $\mathbf{CSH}_{\mathrm{FAT}\ +\ \mathrm{RIND}\ +\ \mathrm{FATXRIND}}$ matrix (B).

factors have a significant effect. In particular, fat content of the pulp and rind percentage generally showed the greatest effect on the spectral response. When considering the AS dataset their effect was comparable, while for the CSH dataset rind percentage showed a higher effect with respect to fat content. However, the variance retained by the ASCA residuals matrix was higher in the model calculated on the CSH dataset with respect to the model calculated on the AS dataset. This fact suggests that the CSH signals are more influenced by the natural variability between different P-R cheese wheels, that was considered in the ASCA models as residual variability.

Therefore, with the future perspective of developing robust calibration models able to predict rind percentage from NIR hyperspectral images of grated P-R cheese, the results of this study suggest that it is not possible to ignore the influence of the considered factors and of the artisanal nature of this food product. In turn, this requires the extensive analysis of a large amount of cheese wheels coming from different dairy factories. Furthermore, since AS and CSH approaches retain complementary information about the hyperspectral images, these two data dimensionality reduction strategies can be coupled through data fusion methods to enhance the performance of the estimate of rind percentage.

CRediT authorship contribution statement

R. Calvini: Methodology, Investigation, Software, Formal analysis, Writing – original draft, Writing – review & editing. **S. Michelini:** Conceptualization, Validation, Data curation, Resources, Writing – review & editing. **V. Pizzamiglio:** Conceptualization, Validation, Resources, Supervision, Writing – review & editing. **G. Foca:** Investigation, Writing – review & editing. **A. Ulrici:** Conceptualization, Methodology, Supervision, Writing – review & editing, Funding acquisition, Project administration.

Declaration of competing interest

The authors declare that they have no conflict of interest.

Acknowledgements

The authors wish to thank Consorzio del Formaggio Parmigiano Reggiano for providing technical and financial support.

References

Alinovi, M., Mucchetti, G., & Tidona, F. (2019). Application of NIR spectroscopy and image analysis for the characterisation of grated Parmigiano-Reggiano cheese. *International Dairy Journal, 92*, 50–58.

Amigo, J. M., Babamoradi, H., & Elcoroaristizabal, S. (2015). Hyperspectral image analysis. A tutorial. *Analytica Chimica Acta, 896*, 34–51.

Bertinetto, C., Engel, J., & Jansen, J. (2020). ANOVA simultaneous component analysis: A tutorial review. *Analytica Chimica Acta, X*, 100061.

Bonifazi, G., Capobianco, G., & Serranti, S. (2018). A hierarchical classification approach for recognition of low-density (LDPE) and high-density polyethylene (HDPE) in mixed plastic waste based on short-wave infrared (SWIR) hyperspectral imaging. *Spectrochimica Acta Part A: Molecular and Biomolecular Spectroscopy, 198*, 115–122.

Burns, D. A., & Ciurczak, E. W. (2008). *Handbook of near infrared analysis*. Boca Raton, Florida, USA: CRC Press. https://doi.org/10.1201/9781420007374

Caballero, D., Calvini, R., & Amigo, J. M. (2020). Hyperspectral imaging in crop fields: Precision agriculture. In *Data handling in science and technology* (Vol. 32, pp. 453–473). Elsevier.

Calvini, R., Foca, G., & Ulrici, A. (2016). Data dimensionality reduction and data fusion for fast characterization of green coffee samples using hyperspectral sensors. *Analytical and Bioanalytical Chemistry, 408*(26), 7351–7366.

Calvini, R., Michelini, S., Pizzamiglio, V., Foca, G., & Ulrici, A. (2020). Exploring the potential of NIR hyperspectral imaging for automated quantification of rind amount in grated Parmigiano Reggiano cheese. *Food Control, 112*, 107111.

Calvini, R., Orlandi, G., Foca, G., & Ulrici, A. (2018). Development of a classification algorithm for efficient handling of multiple classes in sorting systems based on hyperspectral imaging. *Journal of Spectral Imaging, 7*, a13.

Calvini, R., Orlandi, G., Foca, G., & Ulrici, A. (2020). Colourgrams GUI: A graphical user-friendly interface for the analysis of large datasets of RGB images. *Chemometrics and Intelligent Laboratory Systems, 196*, 103915. https://doi.org/10.1016/j.chemolab.2019.103915

Calvini, R., Ulrici, A., & Amigo, J. M. (2020). Growing applications of hyperspectral and multispectral imaging. In *Data handling in science and technology* (Vol. 32, pp. 605–629). Elsevier.

Campbell, G. M., Fang, C., & Muhamad, I. I. (2007). On predicting roller milling performance VI: Effect of kernel hardness and shape on the particle size distribution from first break milling of wheat. *Food and Bioproducts Processing, 85*(1), 7–23.

Cevoli, C., Gori, A., Nocetti, M., Cuibus, L., Caboni, M. F., & Fabbri, A. (2013). FT-NIR and FT-MIR spectroscopy to discriminate competitors, non compliance and compliance grated Parmigiano Reggiano cheese. *Food Research International, 52*(1), 214–220.

Cevoli, C., Ragni, L., Iaccheri, E., Gori, A., Caboni, M. F., Guarnieri, A., & Berardinelli, A. (2015). Estimation of the main compositional features of grated Parmigiano Reggiano cheese by a simple capacitive technique. *Journal of Food Engineering, 149*, 181–187.

Corti, M., Gallina, P. M., Cavalli, D., & Cabassi, G. (2017). Hyperspectral imaging of spinach canopy under combined water and nitrogen stress to estimate biomass, water, and nitrogen content. *Biosystems Engineering, 158*, 38–50.

De Luca, S., De Filippis, M., Bucci, R., Magrì, A. D., Magrì, A. L., & Marini, F. (2016). Characterization of the effects of different roasting conditions on coffee samples of different geographical origins by HPLC-DAD, NIR and chemometrics. *Microchemical Journal, 129*, 348–361.

Duchesne, C., Liu, J. J., & MacGregor, J. F. (2012). Multivariate image analysis in the process industries: A review. *Chemometrics and Intelligent Laboratory Systems, 117*, 116–128.

Ferrari, C., Foca, G., Calvini, R., & Ulrici, A. (2015). Fast exploration and classification of large hyperspectral image datasets for early bruise detection on apples. *Chemometrics and Intelligent Laboratory Systems, 146*, 108–119.

Ferrari, C., Foca, G., & Ulrici, A. (2013). Handling large datasets of hyperspectral images: Reducing data size without loss of useful information. *Analytica Chimica Acta, 802*, 29–39.

Gowen, A. A., O'Donnell, C. P., Cullen, P. J., Downey, G., & Frias, J. M. (2007). Hyperspectral imaging–an emerging process analytical tool for food quality and safety control. *Trends in Food Science & Technology, 18*(12), 590–598.

Gowen, A. A., O'donnell, C. P., Cullen, P. J., & Bell, S. E. J. (2008). Recent applications of chemical imaging to pharmaceutical process monitoring and quality control. *European Journal of Pharmaceutics and Biopharmaceutics, 69*(1), 10–22.

Granato, D., & de Araújo Calado, V. M. (2014). The use and importance of design of experiments (DOE) in process modelling in food science and technology. In D. Granato, & G. Ares (Eds.), *Mathematical and statistical methods in food science and technology, Chpt 1* pp. 1–18). Chicago (USA): John Wiley & Sons. https://doi.org/10.1002/9781118434635.ch1.

Guinee, T. P., Auty, M. A., & Fenelon, M. A. (2000). The effect of fat content on the rheology, microstructure and heat-induced functional characteristics of Cheddar cheese. *International Dairy Journal, 10*(4), 277–288.

Haddad, Y., Mabille, F., Mermet, A., Abecassis, J., & Benet, J. C. (1999). Rheological properties of wheat endosperm with a view on grinding behaviour. *Powder Technology, 105*(1–3), 89–94.

Huang, H., Liu, L., & Ngadi, M. O. (2014). Recent developments in hyperspectral imaging for assessment of food quality and safety. *Sensors, 14*(4), 7248–7276.

Jansen, J. J., Hoefsloot, H. C., van der Greef, J., Timmerman, M. E., Westerhuis, J. A., & Smilde, A. K. (2005). ASCA: Analysis of multivariate data obtained from an experimental design. *Journal of Chemometrics: A Journal of the Chemometrics Society, 19*(9), 469–481.

Kucheryavskiy, S. (2013). A new approach for discrimination of objects on hyperspectral images. *Chemometrics and Intelligent Laboratory Systems, 120*, 126–135.

Lei, T., & Sun, D. W. (2019). Developments of nondestructive techniques for evaluating quality attributes of cheeses: A review. *Trends in Food Science & Technology, 88*, 527–542.

Li Vigni, M., Durante, C., Michelini, S., Nocetti, M., & Cocchi, M. (2020). Preliminary assessment of Parmigiano Reggiano authenticity by handheld Raman spectroscopy. *Foods, 9*(11), 1563.

Lorente, D., Aleixos, N., Gómez-Sanchis, J. U. A. N., Cubero, S., García-Navarrete, O. L., & Blasco, J. (2012). Recent advances and applications of hyperspectral imaging for fruit and vegetable quality assessment. *Food and Bioprocess Technology, 5*(4), 1121–1142.

Malacarne, M., Summer, A., Franceschi, P., Formaggioni, P., Pecorari, M., Panari, G., & Mariani, P. (2009). Free fatty acid profile of parmigiano–reggiano cheese throughout ripening: Comparison between the inner and outer regions of the wheel. *International Dairy Journal, 19*(10), 637–641.

Malegori, C., Oliveri, P., Mustorgi, E., Boggiani, M. A., Pastorini, G., & Casale, M. (2021). An in-depth study of cheese ripening by means of NIR hyperspectral imaging: Spatial mapping of dehydration, proteolysis and lipolysis. *Food Chemistry, 343*, 128547.

Oliveri, P., Malegori, C., Casale, M., Tartacca, E., & Salvatori, G. (2019). An innovative multivariate strategy for HSI-NIR images to automatically detect defects in green coffee. *Talanta, 199*, 270–276.

Ozaki, Y. (2002). Two dimensional near-infrared correlation spectroscopy. In H. W. Siesler, Y. Ozaki, S. Kawata, & M. Heise (Eds.), *Applications in chemistry in near-infrared spectroscopy: Principles, instruments and applications*. Weinheim, Germany: Wiley-VCH, ISBN 978-3-527-30149-2.

Panari, G., Mariani, P., Summer, A., Guidetti, R., & Pecorari, M. (2003). Variazione della composizione e andamento della proteolisi del Parmigiano-Reggiano nel corso della maturazione in riferimento al profilo (centro e periferia) della forma. *Scienza e Tecnica Lattiero Casearia, 54*, 199–212.

Paulrud, S., Mattsson, J. E., & Nilsson, C. (2002). Particle and handling characteristics of wood fuel powder: Effects of different mills. *Fuel Processing Technology, 76*(1), 23–39.

Prats-Montalbán, J. M., De Juan, A., & Ferrer, A. (2011). Multivariate image analysis: A review with applications. *Chemometrics and Intelligent Laboratory Systems, 107*(1), 1–23.

Priyashantha, H., Höjer, A., Saedén, K. H., Lundh, Å., Johansson, M., Bernes, G., Geladi, P., & Hetta, M. (2020). Use of near-infrared hyperspectral (NIR-HS) imaging to visualize and model the maturity of long-ripening hard cheeses. *Journal of Food Engineering, 264*, 109687.

Rogers, N. R., McMahon, D. J., Daubert, C. R., Berry, T. K., & Foegeding, E. A. (2010). Rheological properties and microstructure of Cheddar cheese made with different fat contents. *Journal of Dairy Science, 93*(10), 4565–4576.

Roggo, Y., Edmond, A., Chalus, P., & Ulmschneider, M. (2005). Infrared hyperspectral imaging for qualitative analysis of pharmaceutical solid forms. *Analytica Chimica Acta, 535*(1–2), 79–87.

Šašić, S., & Ozaki, Y. (2000). Band assignment of near-infrared spectra of milk by use of partial least-squares regression. *Applied Spectroscopy, 54*(9), 1327–1338.

Shan, J., Zhang, Y., Liang, J., & Wang, X. (2020). Characterization of the processing conditions upon textural profile Analysis (TPA) parameters of processed cheese using near-infrared hyperspectral imaging. *Analytical Letters, 53*(8), 1190–1203.

Smilde, A. K., Jansen, J. J., Hoefsloot, H. C., Lamers, R. J. A., Van Der Greef, J., & Timmerman, M. E. (2005). ANOVA-simultaneous component analysis (ASCA): A new tool for analyzing designed metabolomics data. *Bioinformatics, 21*(13), 3043–3048.

Specifications of Parmigiano Reggiano Cheese. https://www.parmigianoreggiano.com/consortium/rules_regulation_2/default.aspx.

Ulrici, A., Serranti, S., Ferrari, C., Cesare, D., Foca, G., & Bonifazi, G. (2013). Efficient chemometric strategies for PET–PLA discrimination in recycling plants using hyperspectral imaging. *Chemometrics and Intelligent Laboratory Systems, 122*, 31–39.

Van Den Boomgaard, R., & Van Balen, R. (1992). Methods for fast morphological image transforms using bitmapped binary images. *CVGIP: Graphical Models and Image Processing, 54*(3), 252–258.

Wu, D., & Sun, D. W. (2013). Advanced applications of hyperspectral imaging technology for food quality and safety analysis and assessment: A review—Part II: Applications. *Innovative Food Science & Emerging Technologies, 19*, 15–28.

Xu, J. L., Riccioli, C., & Sun, D. W. (2016). Efficient integration of particle analysis in hyperspectral imaging for rapid assessment of oxidative degradation in salmon fillet. *Journal of Food Engineering, 169*, 259–271.

Zwanenburg, G., Hoefsloot, H. C., Westerhuis, J. A., Jansen, J. J., & Smilde, A. K. (2011). ANOVA–principal component analysis and ANOVA–simultaneous component analysis: A comparison. *Journal of Chemometrics, 25*(10), 561–567.